Short-range order and near-field effects on optical scattering and structural coloration

S. F. Liew,[1,*] J. Forster,[2] H. Noh,[1] C. F. Schreck,[3] V. Saranathan,[4] X. Lu,[5] L. Yang,[6] Richard O. Prum,[4] C. S. O'Hern,[2,3] E. R. Dufresne,[2,3,7,8] and H. Cao[1,3]

[1]*Department of Applied Physics, Yale University, New Haven, Connecticut 06511, USA*
[2]*Department of Mechanical Engineering and Materials Science, Yale University, New Haven, Connecticut 06511, USA*
[3]*Department of Physics, Yale University, New Haven, Connecticut 06511, USA*
[4]*Department of Ecology and Evolutionary Biology, Peabody Museum of Natural History, Yale University, New Haven, Connecticut 06511, USA*
[5]*Department of Condensed Matter Physics and Materials Science, Brookhaven National Laboratory, Upton, New York 11973, USA*
[6]*National Synchrotron Light Source, Brookhaven National Laboratory, Upton, New York 11973, USA*
[7]*Department of Chemical Engineering, Yale University, New Haven, Connecticut 06511, USA*
[8]*Department of Cell Biology, Yale University, New Haven, Connecticut 06511, USA*
**sengfatt.liew@yale.edu*

Abstract: We have investigated wavelength-dependent light scattering in biomimetic structures with short-range order. Coherent backscattering experiments are performed to measure the transport mean free path over a wide wavelength range. Overall scattering strength is reduced significantly due to short-range order and near-field effects. Our analysis explains why single scattering of light is dominant over multiple scattering in similar biological structures and is responsible for color generation.

OCIS codes: (290.1350) Backscattering; (160.4236) Nanomaterials; (350.4238) Nanophotonics and photonic crystals.

References and links

1. P. Vukusic and J. R. Sambles, "Photonic structures in biology," Nature **424**, 852–855 (2003).
2. S. Kinoshita, S. Yoshioka, and J. Miyazaki, "Physics of structural colors," Rep. Prog. Phys. **71**, 076401 (2008).
3. R. O. Prum, R. H. Torres, S. Williamson, and J. Dyck, "Coherent light scattering by blue bird feather barbs," Nature **396**, 28–29 (1998).
4. E. R. Dufresne, H. Noh, V. Saranathan, S. G. J. Mochrie, H. Cao, and R. O. Prum, "Self-assembly of amorphous biophotonic nanostructures by phase separation," Soft Matter **5**, 1792–1795 (2009).
5. B. Q. Dong, X. H. Liu, T. R. Zhan, L. P. Jiang, H. W. Yin, F. Liu, and J. Zi, "Structural coloration and photonic pseudogap in natural random close-packing photonic structures," Opt. Express **18**, 14430–14438 (2010).
6. H. Noh, S. F. Liew, V. Saranathan, R. O. Prum, S. G. J. Mochrie, E. R. Dufresne, and H. Cao, "How non-iridescent colors are generated by quasi-ordered structures of bird feathers," Adv. Mater. **22**, 2871–2880 (2010).
7. J. D. Forster, H. Noh, S. F. Liew, V. Saranathan, C. F. Schreck, L. Yang, J.-G. Park, R. O. Prum, S. G. J. Mochrie, C. S. O'Hern, H. Cao, and E. R. Dufresne, "Biomimetic isotropic nanostructures for structural coloration," Adv. Mater. **22**, 2939–2944 (2010).
8. M. H. Ur-Rashid, A. B. Imran, T. Seki, M. Ishii, H. Nakamura, and Y. Takeoka, "Angle-independent structural color in colloidal amorphous arrays," Chemphyschem **11**, 579–583 (2010).
9. Y. Takeoka, M. Honda, T. Seki, M. Ishii, and H. Nakamura, "Structural colored liquid membrane without angle dependence," ACS Appl. Mater. Interfaces **1**, 982–986 (2009).

#142190 - $15.00 USD Received 7 Feb 2011; accepted 28 Mar 2011; published 14 Apr 2011

10. K. Ueno, A. Inaba, Y. Sano, M. Kondoh, and M. Watanabe, "A soft glassy colloidal array in ionic liquid, which exhibits homogenous, non-brilliant and angle-independent structural colors," Chem. Commun. 3603–3605 (2009).
11. I. Lee, D. Kim, J. Kal, H. Baek, D. Kwak, D. Go, E. Kim, C. Kang, J. Chung, Y. Jang, S. Ji, J. Joo, and Y. Kang, "Quasi-amorphous colloidal structures for electrically tunable full-color photonic pixels with angle-independency," Adv. Mater. **22**, 4973–4977 (2010).
12. H. Noh, S. F. Liew, V. Saranathan, R. O. Prum, S. G. J. Mochrie, E. R. Dufresne, and H. Cao, "Double scattering of light from biophotonic nanostructures with short-range order," Opt. Express **18**, 11942–11948 (2010).
13. H. Noh, S. F. Liew, V. Saranathan, R. O. Prum, S. G. J. Mochrie, E. R. Dufresne, and H. Cao, "Contribution of double scattering to structural coloration in quasi-ordered nanostructures of bird feathers," Phys. Rev. E **81**, 051923 (2010).
14. S. Torquato, T. M. Truskett, and P. G. Debenedetti, "Is random close packing of spheres well defined?,"Phys. Rev. Lett. **84**, 2064–2067 (2000).
15. J. G. Berryman, "Random close packing of hard spheres and disks," Phys. Rev. A **27**, 1053–1061 (1983).
16. E. Akkermans and G. Montambaux, *Mesoscopic Physics of Electrons and Photons* (Cambridge University Press, 2007).
17. C. F. Schreck and C. S. O'Hern, "Computational methods to study jammed systems," in *Experimental and Computational Techniques in Soft Condensed Matter Physics*, ed. by J. S. Olafsen, (Cambridge University Press, 2010).
18. Y. Chonde and I. M. Krieger, "Emulsion polymerization of styrene with ionic comonomer in the presence of methanol," J. Appl. Polymer Sci. **26**, 1819–1827 (1981).
19. S. Fraden and G. Maret, "Multiple light scattering from concentrated, interacting suspensions," Phys. Rev. Lett. **65**, 512–515 (1990).
20. L. Blum and G. J. Stell, "Scattering function for polydisperse fluids of hard or permeable spheres," J. Chem. Phys. **71**, 42–46 (1979).
21. W. L. Griffith, R. Triolo, and A. L. Compere, "Analytical scattering function of a polydisperse Percus-Yevick fluid with Schulz -(Γ-) distributed diameters," Phys. Rev. A **35**, 2200–2206 (1987).
22. Y. Huang, Z. Sun, and E. M. Sevick-Muraca, "Assessment of electrostatic interactions in dense colloidal suspensions with multiply scattered light," Langmuir **18**, 2048–2053 (2002).
23. H. C. van de Hulst, *Light Scattering by Small Particles* (Dover, 1981).
24. C. S. O'Hern, L. E. Silbert, A. J. Liu, and S. R. Nagel, "Jamming at zero temperature and zero applied stress: the epitome of disorder," Phys. Rev. E **68**, 011306 (2003).
25. G.-J. Gao, J. Blawzdziewicz, and C. S. O'Hern, "Frequency distribution of mechanically stable disk packings," Phys. Rev. E **74**, 061304 (2006).
26. L. F. Rojas-Ochoa, J. M. Mendez-Alcaraz, J. J. Sáenz, P. Schurtenberger, and F. Scheffold, "Photonic properties of strongly correlated colloidal liquids," Phys. Rev. Lett. **93**, 073903 (2004).
27. R. W. Hart and R. A. Farrell, "Light scattering in the cornea," J. Opt. Soc. Am. **59**, 766–773 (1969).
28. X. T. Peng and A. D. Dinsmore, "Light propagation in strongly scattering, random colloidal films: the role of the packing geometry," Phys. Rev. Lett. **99**, 143902 (2007).
29. L. E. McNeil and R. H. French, "Multiple scattering from rutile TiO2 particles," Acta Mater. **48**, 4571–4576 (2000).
30. E. V. Petrova, V.P. Tishkovets, and K. Jockers, "Interaction of particles in the near field and opposition effects in regolith-like surfaces," Solar Syst. Res. **43**, 100–115 (2009).
31. A. F. Koenderink, M. Megens, G. van Soest, W. L. Vos and A. Lagendijk, "Enhanced backscattering from photonic crystals," Phys. Lett. A **268**, 104–111 (2000).
32. J. Huang, N. Eradat, M. E. Raikh, and Z. V. Vardeny, "Anomalous coherent backscattering of light from optical photonic crystals," Phys. Rev. Lett. **86**, 4815–4818 (2001).
33. A. F. Koenderink, A. Lagendijk, and W. L. Vos, "Optical extinction due to intrinsic structural variations of photonic crystals," Phys. Rev. B **72**, 153102 (2005).
34. P. D. García, R. Sapienza, L. S. Froufe-Pérez, and C. López, "Strong dispersive effects in the light-scattering mean free path in photonic gaps," Phys. Rev. B **79**, 241109 (2009).

1. Introduction

Structural color, which has been widely employed in nature, originates from light scattering by nanostructures with spatial variation in the refractive index on the scale of optical wavelengths. The most studied examples are periodic structures that produce iridescent color via Bragg scattering [1, 2]. In recent years, there is a growing interest in the previously unappreciated class of quasi-ordered structures that can generate non-iridescent color [3–7]. Such structures have only short-range order and are isotropic, making color invariant with viewing angle in natural lighting conditions. Biomimetic samples have been fabricated by self-assembly of colloidal

#142190 - $15.00 USD Received 7 Feb 2011; accepted 28 Mar 2011; published 14 Apr 2011

particles [7, 8], and have potential applications in wide-angle color displays [9–11].

We recently studied the mechanism of coloration of quasi-ordered nanostructures in feather barbs of many bird species [4]. Single scattering of light [6], with contributions from double scattering [12, 13], is shown to determine the color. The angular dispersion and polarization characteristic of the major/secondary peak in the scattering spectra agree well to the predictions of single/double scattering. Local structural correlation leads to strong backward scattering of light within a narrow frequency range, which is selected by the characteristic length scale of the structure. A puzzle left from our previous study is why only low-order scattering events are observed from those structures even though simple estimations of scattering length would predict strong multiple scattering. As an example, Fig. 1(a) shows part of a cross-sectional transmission electron micrograph (TEM) of the feather barb of *Cotinga maynana* (a blue green bird). The nanostructured layer underneath the cortex is about 10 μm thick, and consists of random close-packed [14, 15] spherical air cavities in a β-keratin matrix. The transport mean free path l_t of light in this structure, assuming independent scattering approximation, is significantly smaller than the thickness of the nanostructured layer. Thus, one might expect that multiple scattering to dominate over single scattering and remove wavelength dependence in the reflection spectrum. However, such structures create vivid colors in reflection as shown in Ref. [4]. The dominant peak in the optical scattering spectrum coincides with the X-ray scattering peak, confirming the former is from single scattering of light [6].

To resolve this puzzle, we have directly measured the transport mean free path l_t in biomimetic samples, which are made of random close-packed dielectric spheres in air [Fig. 1(b)]. The reason we use biomimetic samples instead of biological samples is that the nanostructured layers in the latter [Fig. 1(a)] are too thin for the coherent backscattering (CBS) experiment which we perform to extract l_t [16]. We find an order of magnitude difference between the measured value of l_t and the estimated one over a broad frequency range. Our theoretical analysis reveals that short-range order and near-field effects reduce the overall (angle-integrated) scattering strength and increase l_t dramatically. Thus, in the biological samples which have similar scattering strength as the biomimetic samples, the transport mean free path is comparable to the thickness of nanostructured layer. Consequently, single scattering is much stronger than multiple scattering, and dominates coloration.

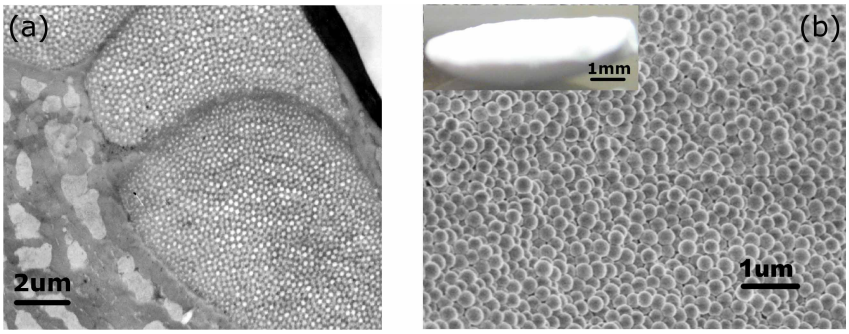

Fig. 1. (a) Transmission electron micrograph (TEM) showing the amorphous photonic structure (right part) in a feather barb of *Cotinga maynana* that produces blue color. Uniform spherical air cavities (white) are closely packed in β-keratin (grey). The structure is isotropic and has only short-range order. (b) Scanning electron micrograph (SEM) of our biomimetic sample made of random close-packed polystyrene spheres of two sizes. Inset is a photo image of the entire sample.

#142190 - $15.00 USD Received 7 Feb 2011; accepted 28 Mar 2011; published 14 Apr 2011

2. Measurement of transport mean free path

To avoid polycrystalline structures that can be easily formed with monodisperse spheres, we fabricate the biomimetic samples by self-assembly of bi-disperse spheres of polystyrene [17]. First, the monodisperse spheres are synthesized using a surfactant-free polymerization technique [7, 18]. The sphere size can be varied by changing the methanol concentration. Then, equal volumes of monodisperse suspensions with polydispersity of 2% are mixed to make a bi-disperse suspension. An approximate 0.5 mL droplet of this bi-disperse suspension is pipetted into a 5 cm diameter petri dish containing 5 mL of Fluorinert FC-70. The suspension droplet is almost completely surrounded by Fluorinert, allowing slow evaporation of water. After all the water has evaporated from the suspension, the sample is removed from Fluorinert, and placed on a Kimwipe to allow any residual Fluorinert to drain from the sample. The final sample has a dome shape [inset of Fig. 1(b)]. The maximum thickness at the center is about 1 mm, much larger than the thickness of nanostructured layers in bird feather barbs [Fig. 1(a)].

Figure 1(b) is a scanning electron micrograph (SEM) taken from the interior surface of a cracked sample. It shows the polystyrene spheres are random close-packed. This structure is the inverse of that with air spheres in the bird feather [Fig. 1(a)]. It also resembles the color-producing structures made of dielectric spheres in some species of beetles [5]. We have performed small-angle X-ray scattering (SAXS) measurement on the sample for quantitative structural characterization. The SAXS data yield a diffused ring pattern as shown in the inset of Fig. 2(a), indicating the structure is isotropic. Azimuthal-averaged SAXS intensity (black solid curve) in Fig. 2(a) reveals that our structure has a dominant spatial frequency q_o = 0.03 nm^{-1}. The corresponding spatial periodicity is $a = 2\pi/q_o$ = 210 nm. The form factor of monodisperse spheres causes regular oscillation of SAXS intensity at large q value, where the structure factor diminishes. Since our sample has bi-disperse spheres, there are two oscillations with slightly different periods. Their beating can be clearly seen in Fig. 2(b) (black solid curve). By fitting the oscillation and beating of the SAXS intensity with the analytical expression of form factors [red dashed line in Fig. 2(b)], the diameters of two spheres are found to be 223 nm and 265 nm respectively.

To characterize the scattering properties of our biomimetic samples, we have performed coherent backscattering (CBS) experiment to obtain the transport mean free path l_t as a function of wavelength λ. A supercontinuum light source is used to cover a broad range of λ from 520 nm to 700 nm. Beyond this range, several lasers with operation wavelengths of 406 nm, 445 nm, and 473 nm are used to probe scattering at shorter λ. Supercontinuum light is generated in a photonic crystal fiber by femtosecond pulses from a mode-locked Ti:Sapphire laser (pulse width $\sim$ 200 fs, repetition rate 76 MHz). The output beam is dispersed by a diffraction grating, and a slit picks light at certain wavelength (with a bandwidth of 5 nm). The filtered light is collimated and incident on the sample after passing through a linear polarizer. The illumination spot on the sample surface is about 2 mm in diameter. The sample is tilted in such a way that the surface reflection of the incident beam deviates from the backscattering direction.

The scattered light with polarization parallel to the incident one is detected by a photomultiplier tube. An optical chopper and a lock-in amplifier are used to enhance the signal to noise ratio. The scattered light intensity I_s is measured as a function of angle θ_B from the backscattering direction. The sample is rotated during the measurement to smear out the speckle pattern. Figure 3(a) shows the measured $I_s(\theta_B)$ at λ = 473 nm, 580 nm and 660 nm. As λ increases, the CBS cone becomes narrower, indicating l_t is longer. The measured $I_s(\theta_B)$ is fitted by the analytical expression of CBS intensity [16], taking into account the finite angular resolution $\delta\theta$ of the experimental apparatus. By replacing the scattering sample with a highly-reflective mirror, we determine $\delta\theta \simeq 0.6$ mrad. Fitting parameters for $I_s(\theta_B)$ are the enhancement factor, the constant background from single scattering, and the transport mean free path l_t. By repeating

#142190 - $15.00 USD Received 7 Feb 2011; accepted 28 Mar 2011; published 14 Apr 2011

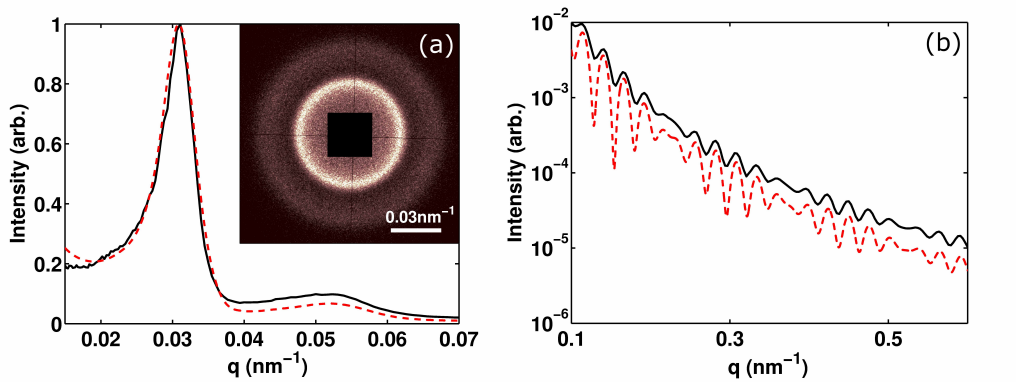

Fig. 2. Small Angle X-ray Scattering (SAXS) measurement of the biomimetic sample. (a) SAXS pattern (inset) showing an isotropic ring pattern. The azimuthal-averaged SAXS intensity (black solid line in main panel) reveals the existence of a dominant spatial frequency in the structure. The red-dashed curve is obtained from the power Fourier spectrum of a computer-simulated structure shown in Fig. 4(a). (b) Log-linear plot of SAXS intensity (black solid line) at high q value featuring the oscillation and beating, caused by the form factors of bi-disperse spheres. Red dashed curve is from the calculation with form factors of two spheres with diameters 265 nm and 223 nm. The red dashed curve is shifted vertically for better comparison.

the CBS measurement at many wavelengths, we obtain l_t as a function of λ [black squares in Fig. 3(b)]. The fitting error for all data points are below 5%.

3. Theoretical analysis

To interpret the experimental data, we estimate $l_t = (\rho\sigma_t)^{-1}$ from the transport cross section σ_t [19],

$$\sigma_t = \frac{\pi}{k^2}\int_0^{\pi} B(\theta)\sin\theta(1-\cos\theta)d\theta, \tag{1}$$

where

$$B(\theta) = xF_{11}(\theta)S_{11}(\theta)+(1-x)F_{22}(\theta)S_{22}(\theta)+2\sqrt{x(1-x)}F_{12}(\theta)S_{12}(\theta). \tag{2}$$

The partial structure factors for the bi-disperse system are

$$S_{11}(q) = \frac{1}{\sqrt{N_1N_1}}\langle\sum_{n,m} e^{i\mathbf{q}\cdot(\mathbf{r}_n^{(1)}-\mathbf{r}_m^{(1)})}\rangle - \sqrt{N_1N_1}\delta(q), \tag{3}$$

$$S_{22}(q) = \frac{1}{\sqrt{N_2N_2}}\langle\sum_{n,m} e^{i\mathbf{q}\cdot(\mathbf{r}_n^{(2)}-\mathbf{r}_m^{(2)})}\rangle - \sqrt{N_2N_2}\delta(q), \tag{4}$$

$$S_{12}(q) = \frac{1}{\sqrt{N_1N_2}}\langle\sum_{n,m} e^{i\mathbf{q}\cdot(\mathbf{r}_n^{(1)}-\mathbf{r}_m^{(2)})}\rangle - \sqrt{N_1N_2}\delta(q). \tag{5}$$

The binary form factors are $F_{11} = f_{s,1}f_{s,1}^* + f_{p,1}f_{p,1}^*$, $F_{22} = f_{s,2}f_{s,2}^* + f_{p,2}f_{p,2}^*$, and $F_{12} = Re[f_{s,1}f_{s,2}^* + f_{p,1}f_{p,2}^*]$ [20–22]. Particles with diameter 265 nm are labeled as 1, and 223 nm as 2. N_1 and N_2 denote the numbers of larger and smaller particles respectively. $x = N_1/(N_1+N_2)$ is the fraction of larger particles in the mixture, which is 0.4 in our sample. f_s and f_p are the

#142190 - $15.00 USD Received 7 Feb 2011; accepted 28 Mar 2011; published 14 Apr 2011

scattering amplitudes of two orthogonal polarizations from a spherical particle, which can be calculated by Mie scattering theory [23]. $k = 2\pi n_{eff}/\lambda_o$ is the scattering wave vector, where n_{eff} is the effective refractive index of the scattering medium. $q = 2k\sin(\theta/2)$ is the spatial frequency, where θ is the scattering angle ranging from 0° in the forward direction to 180° in the backward direction. The particle density is $\rho = \phi/[xv_1 + (1-x)v_2]$, where v_1 and v_2 are the volumes of particles with diameter 265 nm and 223 nm respectively.

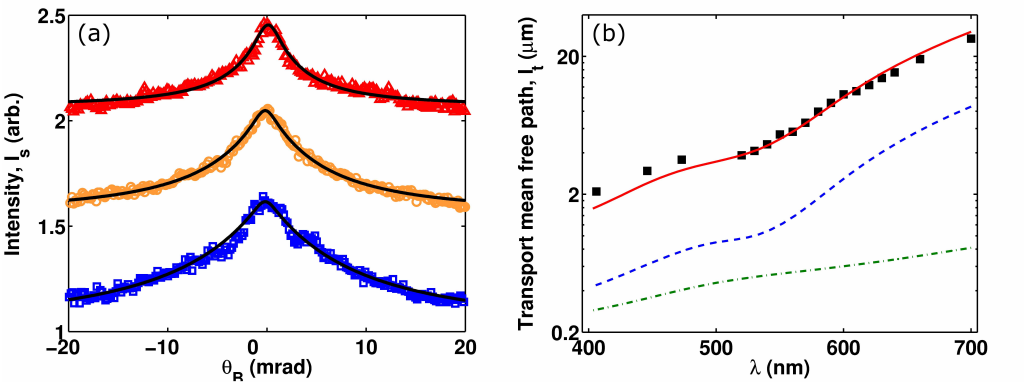

Fig. 3. (a) Coherent backscattering (CBS) measurement (a) CBS intensity I_s vs. scattering angle θ_B, measured at λ = 660 nm (red triangle), 580 nm (orange circle) and 473 nm (blue square). $\theta_B = 0$ in the backscattering direction. Black solid lines represent the fitted curves. (b) Measured (black square) and estimated (lines) transport mean free path l_t vs. wavelength λ. Green dash-dots curve represents l_t estimated without short-range order and near-field effects, blue dashed line is with short-range order but no near-field effects, and red solid curve is with both.

We start with a simple estimation of l_t in our sample with two assumptions. First, we assume independent scattering of light by individual particles. Secondly, we ignore the short-range order by assuming the particles are randomly located without any correlation, namely, $S_{11} = 1$, $S_{22} = 1$, and $S_{12} = 0$. The dielectric spheres have the refractive index of $n = 1.58$, and the filling fraction of $\phi = 64\%$ [24]. The form factors are calculated from optical scattering of individual dielectric spheres in air. The computed value of l_t is plotted by the green dash-dotted line in Fig. 3(b).

Next, we take into account local correlation of particle position in the random close-packed structure by including the structure factors of the bi-disperse system in the estimation of l_t. However, it is very difficult, if not impossible, to accurately extract all partial structure factors S_{11}, S_{22}, and S_{12} from the SAXS data. Alternatively, they are obtained from a computer-simulated random close-packed system of 1000 bi-disperse spheres of diameters equal to the experimental values [Fig. 4(a)] using the methods described in Ref. [25]. The filling fraction is 64% [24]. The partial structure factors are calculated from the center positions of all spheres and plotted in Fig. 4(b). Power Fourier spectrum, computed by Fourier transform of this structure, matches well the azimuthal-averaged SAXS intensity in Fig. 2(a). This agreement confirms that our sample has a filling fraction of 64%, because with identical sphere sizes and number ratio x of bi-disperse spheres, the dominant spatial frequency would coincide only if the filling fraction is the same. The estimated l_t is plotted by the blue dashed line in Fig. 3(b). Its value is increased from the previous estimation as a result of short-range order. This result is a little surprising, as structural correlation is often thought to enhance light scattering, at least, at certain wavelength. Short-range structural order introduces the phase correlation of light scattered by adjacent particles, leading to constructive interference in certain direction and destructive interference in

#142190 - $15.00 USD Received 7 Feb 2011; accepted 28 Mar 2011; published 14 Apr 2011

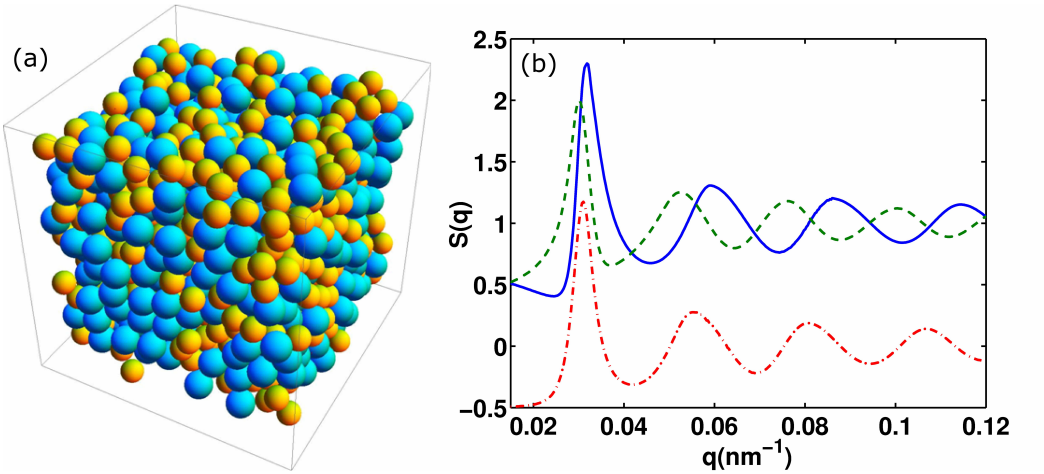

Fig. 4. (a) Computer-simulated structure of random close-packed spheres of diameters 265 nm (blue) and 223 nm (yellow). (b) Partial structure factors computed for the structure in (a). Blue solid curve is S_{11}, green dashed curve S_{22}, and red dash-dots curve S_{12}.

other directions. To be more concrete, let us consider light with an incident wave vector $\mathbf{k}_i$ being scattered to a wave vector $\mathbf{k}_o$. The scattering is elastic, $|\mathbf{k}_i| = |\mathbf{k}_o| = k$. The difference between $\mathbf{k}_i$ and $\mathbf{k}_o$ is provided by the spatial vector $\mathbf{q}$ of the structure, $\mathbf{k}_o - \mathbf{k}_i = \mathbf{q}$. For example, in the backward scattering direction, $\mathbf{k}_o = -\mathbf{k}_i$, thus $2k = q$. The dominant spatial frequency q_o of the random close-packed system causes the strongest backward scattering at $k = q_o/2$. Consequently, l_t exhibits a shallow "dip" at the corresponding $\lambda \approx 550$ nm [blue dashed line in Fig. 3(b)] [26]. More generally, for any $k > q_o/2$, short-range structural order introduces a phase correlation of light scattered by adjacent particles. They constructively interfere in specific directions, enhancing the scattered light intensity. However, in all other directions they interfere destructively, suppressing light scattering. The suppression of scattering intensity occurs in many more directions than the enhancement. Hence, the total (angle-integrated) scattering strength reduces and l_t increases. It has been shown in Ref. [27] that short-range order reduces scattering and is responsible for the transparency of cornea to visible light. However, in Ref. [27], the characteristic length scale of the nanostructure is about an order of magnitude smaller than the optical wavelength, while in our case they are comparable.

In the above two estimations of l_t, we calculate the form factors by assuming the particles are situated in a background of air. However, in a random close-packed system, particles are in contact with each other, and the scattering cross section of a particle is affected by the presence of nearby particles [28]. The near-field coupling of the adjacent particles modifies the form factor of an "average" particle. Such near-field effects have been reported in the study of white pigmentation using TiO_2 particles [29] and it is called optical crowding. Scattering of solar electromagnetic radiation by dust particles in the atmosphere or on the surface of celestial bodies are also affected by the near-field effects [30]. To take into account the near-field effects in our random close-packed sample, the form factors of particles are computed by assuming each particle is effectively surrounded by a homogeneous dielectric background of refractive index n_b. The value of n_b is obtained by averaging the actual refractive index surrounding a particle with a weighting factor from an exponentially-decaying evanescent field. Namely,

$$n_b = \frac{\int_0^\infty n(r) e^{-\alpha r/\lambda_o} r^2 dr}{\int_0^\infty e^{-\alpha r/\lambda_o} r^2 dr} \tag{6}$$

#142190 - $15.00 USD Received 7 Feb 2011; accepted 28 Mar 2011; published 14 Apr 2011

where r is the distance from a particle's surface, $n(r)$ is the ensemble-averaged refractive index based on on the sphere packings described above, and α is a fitting parameter that we expect to depend on the refractive indices of the particles and the surrounding medium as well as the local particle packing geometry. We can calculate l_t for any value of α using the modified form factors with background refractive index n_b from Eq. (6). The least square fitting between the measured and estimated values of l_t for all probed wavelengths gives $\alpha = 14.1 \pm 3.2$. The relative standard error is $\approx 9\%$. With larger/smaller α value, the magnitude of l_t decreases/increases, but the shape of the curve remain constant. The final estimated l_t which includes the short-range order and near-field effects is plotted by red solid line in Fig. 3(b), and in good agreement with the experimental values at all measured wavelengths. This result indicates that short-range order and near-field effects reduce the scattering strength by one order of magnitude in random close-packed structures.

4. Discussion and conclusion

Although the transport mean free path has been well studied in disordered photonic crystals with long-range order [31–34], there have been only a few studies on amorphous photonic structures with short-range order. It has been shown in colloidal liquids, local order induces a local minimum of the transport mean free path [26]. Since the particles are not closely packed, the near-field effect is negligible. In Ref. [28], l_t is shown to increase at high filling fraction of a random close-packed random film of monodisperse dielectric spheres. This result is explained by accounting for evanescent wave coupling of contacting spheres. The modification of near-field scattering environment is included in the form factors of isolated scatterers in an effective dielectric background. The background refractive index is obtained after setting a coupling length that scales linearly with λ. Following this method, we calculate n_b as a function of wavelength and plot (with blue dashed line) in Fig. 5(a). Its value displays a sharp rise at $\lambda \sim 200$ nm. Within the wavelength range of our study, its value is nearly invariant with λ. The l_t calculated with this background index is roughly 3 times larger than the measured values for our samples (not shown). For comparison, we plot (with black solid line) in Fig. 5(a) the value of n_b obtained from Eq. (6) with $\alpha = 14.1$. It has a much more gradual increase with λ. The background index n_b is notably lower within the wavelength range of our measurement. The good agreement between the estimated l_t with this n_b and the measured values over a broad wavelength range clearly shows that our proposed model works better to incorporate the near-field effects in a random close-packed scattering environment. The asymptotic behavior of n_b can be understood as follows. At longer wavelength, the near-field of a particle would extend farther away, coupling to more particles and probe the global environment. Thus the background refractive index approaches that of a homogenized medium which is $n_h = 1.39$ in our case. In the short-wavelength limit, the particle would only be able to sense its immediate environment and n_b approaches the refractive index of air. As an example, we plot in Fig. 5(b) the scattering efficiency Q_{sca} of a dielectric sphere in different backgrounds. Q_{sca} is defined as the ratio of the total scattering cross section over the geometrical cross section of a sphere. The sphere diameter is 244 nm and the refractive index is 1.58. Q_{sca} calculated with background n_b from Eq. (6) approaches that of scattering in air at short wavelength, and that in homogenized medium of n_h at long wavelength.

Assuming the same α value, we have estimated $l_t \approx 5\mu$m at $\lambda = 540$ nm the center wavelength of the major reflection peak for the nanostructures of bird feather barb as shown in Fig. 1(a). Thus, l_t is comparable to the total thickness of the scattering nanostructures, and single scattering is dominant over multiple scattering to produce color. However, the nanostructures of bird feather barb (air cavities embedded in β-keratin) are inverse of the biomimetic structures (dielectric spheres in air), and the value of α is likely to be different. We expect the α

#142190 - $15.00 USD Received 7 Feb 2011; accepted 28 Mar 2011; published 14 Apr 2011

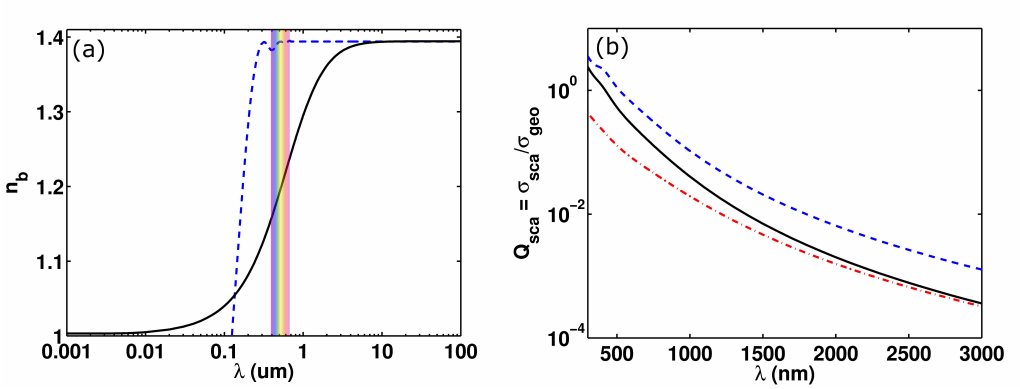

Fig. 5. (a) Near-field effects on form factors can be included in an effective background refractive index n_b, whose value is calculated from Eq. (6). It approaches the refractive index of air at short wavelength, and that of a homogenized medium at long-wavelength. The wavelength range of our CBS measurement is highlighted with color. For comparison, the value of n_b obtained from Ref. [28] is plotted with blue dashed line. (b) Calculated scattering efficiency Q_{sca} of a dielectric sphere in different backgrounds. The sphere has a diameter 244 nm and a refractive index of 1.58. $Q_{sca} = \sigma_{sca}/\sigma_{geo}$ is the ratio of the scattering cross section σ_{sca} to the geometical cross section σ_{geo}. The refractive index of the background is equal to n_b from Eq. (6) (black solid line), $n_h = 1.39$ of the homogenized medium (blue dashed line), and that of air 1 (red dash-dotted line).

value determined in this paper is not universal, since it depends on the properties of the scatterer and its surrounding. It is sensitive to the parameters such as ratio of refractive index of scatterer with its background, size of scatterer and maybe the packing geometry. Hence, further study of light scattering by systematic tuning of the above mentioned parameters has the potential of fully characterizing α, and providing physical insight to dependent scattering.

In summary, we have measured the transport mean free path l_t with coherent backscattering in amorphous photonic structures over a broad wavelength range. Such structures are made of random close-packed dielectric spheres of two sizes, and have only short-range order. The measured l_t is significantly larger than the estimated value based on the assumptions of independent scattering and the absence of structural order. With particles in close contact with one another, we must consider the phase correlation of scattered light and local scattering environment. Short-range order accounts for the interference of light scattered from particles located in close proximity. Near-field effects originate from the evanescent wave coupling of adjacent particles and leads to reduced refractive index contrast between particles and surrounding. Both increase the transport mean free path. Since many color-producing biological nanostructures consist of random close-packed dielectric or air spheres, we expect both effects exist. They increase l_t and make it comparable to the total size of the nanostructure. Consequently, single scattering becomes dominant over multiple scattering, and is responsible for structural coloration.

Acknowledgments

We thank Professor Simon Mochrie for stimulating discussions. This work is supported with seed funding from the Yale NSFMRSEC (DMR-0520495) and NSF grants to HC (PHY-0957680), ERD (CAREER CBET-0547294) and CSOH (DMS-0835742). Use of the National Synchrotron Light Source, Brookhaven National Laboratory, was supported by the U.S. Depart-

ment of Energy, Office of Science, Office of Basic Energy Sciences, under Contract No. DE-AC02-98CH10886. SAXS data were collected with the help of Drs. Alec Sandy and Suresh Narayanan at beamline 8-ID-I of the Advanced Photon Source, Argonne National Labs, and supported by the US Department of Energy, Office of Science, Office of Basic Energy Sciences, under Contract DE-AC02-06CH11357.

#142190 - $15.00 USD Received 7 Feb 2011; accepted 28 Mar 2011; published 14 Apr 2011